

A Geometric Theory of Cognition

Laha Ale^{1,*}

¹Southwest Jiaotong University, School of Computing and Artificial Intelligence, Chengdu, China
 *laha.ale@ieee.org

ABSTRACT

Human cognition spans perception, memory, intuitive judgment, deliberative reasoning, action selection and social inference, yet these capacities are often explained through distinct computational theories. Here we present a unified mathematical framework in which diverse cognitive processes emerge from a single geometric principle. We represent the cognitive state as a point on a differentiable manifold endowed with a learned Riemannian metric that encodes representational constraints, computational costs and structural relations among cognitive variables. A scalar cognitive potential combines predictive accuracy, structural parsimony, task utility and normative or logical requirements. Cognition unfolds as the Riemannian gradient flow of this potential, providing a universal dynamical law from which a broad range of psychological phenomena arise. Classical dual-process effects—rapid intuitive responses and slower deliberative reasoning—emerge naturally from metric-induced anisotropies that generate intrinsic time-scale separations and geometric phase transitions, without invoking modular or hybrid architectures. We derive analytical conditions for these regimes and demonstrate their behavioural signatures through simulations of canonical cognitive tasks. Together, these results establish a geometric foundation for cognition and suggest guiding principles for the development of more general and human-like artificial intelligence systems.

Keywords: Artificial General Intelligence, Cognitive Science

Main

Cognition involves perceiving the world,^{1,2} forming and retrieving memories,^{3,4} acting purposefully,^{5,6} and flexibly shifting between fast intuitive judgments⁷ and slower deliberative reasoning.⁸ Despite substantial progress across neuroscience, psychology and artificial intelligence, these capacities are typically explained through distinct computational traditions, each capturing only a limited facet of the cognitive repertoire.⁹ As a result, there is no shared mathematical description that explains how such diverse processes arise and interact within a single system. The absence of such a unifying framework has constrained efforts to identify the organising principles that underpin intelligent behaviour, in both biological and artificial agents.¹⁰

A central challenge in understanding cognition is that prevailing theories impose strong assumptions on the nature of internal mental representations. Probabilistic accounts characterise cognition as approximate inference,¹¹ neural theories emphasise dynamics in recurrent circuits,^{12,13} symbolic approaches posit discrete, rule-based structures; and contemporary machine-learning models rely on particular function classes, optimisation objectives or architectural constraints. Although these approaches have achieved notable successes, their representational commitments make it difficult to explain how diverse cognitive phenomena—such as intuitive, habitual responses and slower, deliberative reasoning—emerge from shared underlying principles. Dual-process theories describe the coexistence of fast and slow modes of thought,¹⁴ but do not account for why such regimes arise or how they are related within a single computational system.

Here we introduce a geometric principle that unifies diverse cognitive processes within a single mathematical framework, as shown Figure 1. We represent the internal cognitive state as a point on a differentiable manifold whose metric encodes the representational constraints, computational costs and structural dependencies among cognitive variables. Within this space, a scalar cognitive potential combines multiple behavioural drives—including predictive accuracy, representational economy, task utility and normative requirements—into a single quantity that governs internal dynamics. Cognition is then expressed as Riemannian^{15,16} gradient flow on this manifold, yielding a universal dynamical rule that does not depend on specific representational assumptions and applies across perceptual,^{17,18} motor, memory, and reasoning domains.

This geometric formulation explains the emergence of dual-process phenomena. We show analytically that anisotropies in the cognitive metric induce intrinsic separations in time scale: directions of steep curvature support fast, attractor-driven dynamics characteristic of intuitive or habitual responses, whereas shallow directions support slower, exploratory dynamics associated with deliberative reasoning. These regimes arise without modular decomposition or distinct system components; instead, they follow from the intrinsic geometry of cognitive space. Simulations illustrate how these geometric effects generate transitions between intuitive and deliberative modes and reproduce behavioural patterns that are difficult to account for using existing theoretical frameworks.

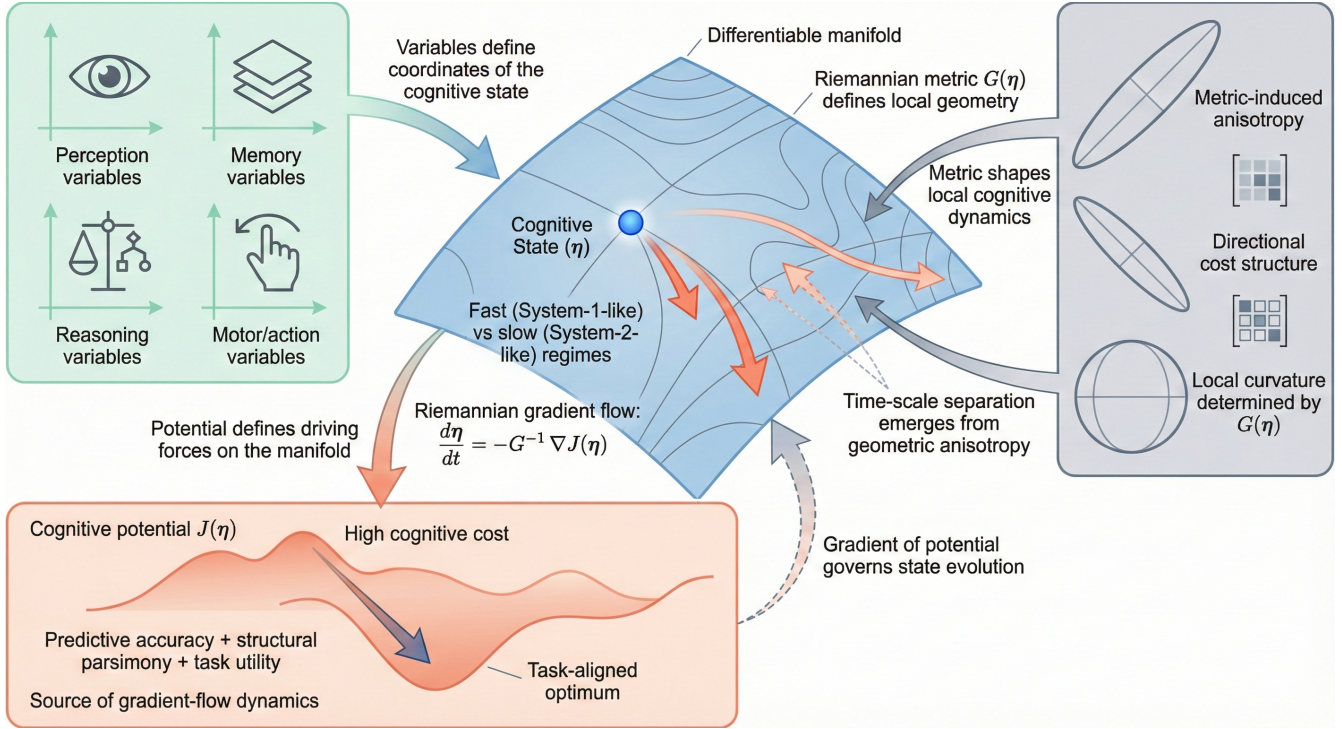


Figure 1. Geometric representation of the cognitive state and its dynamics. The cognitive state is modelled as a point on a differentiable manifold whose geometry captures relationships among perceptual, memory, motor, and reasoning variables. The Riemannian metric encodes representational constraints and computational costs, shaping the local curvature of cognitive space. A cognitive potential integrates predictive, structural and task-related drives into a scalar landscape over the manifold. Cognition unfolds as gradient flow on this landscape, with steep directions producing rapid, intuitive dynamics and shallow directions supporting slower, deliberative exploration. Together, these geometric components provide a unified computational structure from which diverse cognitive regimes emerge.

Together, these results establish a geometric foundation for cognition, showing that a single mathematical principle can generate multiple cognitive regimes and unify previously disparate theories. This framework suggests new links between cognitive science,¹⁹ neuroscience and artificial intelligence, and provides a route toward a general theory of adaptive intelligent behaviour.

2. Gradient-flow formulation of cognition

In this section, we formalise cognition as a gradient flow on a geometric space. We begin by defining the cognitive state, cognitive potential, and Riemannian metric, then present basic properties of the resulting dynamical system.

2.1 Cognitive state and potential

In our formulation, cognition is expressed as the evolution of an internal state driven by the minimisation of a scalar objective. To make this precise, we introduce two basic mathematical objects: the *cognitive state*, which describes the agent's internal configuration at time t , and the *cognitive potential*, a scalar quantity that evaluates the quality, efficiency, or coherence of that configuration.

Definition 1 (Cognitive state and cognitive potential). *The cognitive state at time t is represented by a vector*

$$\eta(t) = (\eta_1(t), \eta_2(t), \dots, \eta_n(t)) \in \mathbb{R}^n,$$

and the cognitive potential is a function

$$J : \mathbb{R}^n \rightarrow \mathbb{R}, \quad \eta \mapsto J(\eta),$$

which we assume to be twice continuously differentiable, $J \in C^2$.

The assumption $J \in C^2$ ensures that both the gradient ∇J and the Hessian $\nabla^2 J$ exist and vary smoothly. This regularity is essential for the framework developed below: gradient-flow dynamics require ∇J ; stability and curvature-based analyses rely on $\nabla^2 J$; and the fast–slow decomposition used to model intuitive versus deliberative cognition depends on smoothness to apply classical geometric singular perturbation theory. Together, these conditions guarantee that the resulting cognitive dynamics are well-defined and amenable to rigorous geometric analysis.

The function $J(\eta)$ assigns a real-valued score to each cognitive state and serves as a global cognitive objective. Its role is analogous to a loss function in machine learning or to a potential-energy landscape in physics, providing a unified quantity that governs the system’s internal dynamics. Crucially, J integrates the diverse pressures that shape cognition into a single scalar potential: prediction accuracy, representational simplicity, decision-theoretic utility, logical or normative consistency, and the resource or computational costs associated with maintaining and transforming internal representations. In the sections that follow, we show how these heterogeneous drives can be expressed within a common geometric framework and how their joint optimisation yields coherent cognitive behaviour.

Cognition involves balancing several competing pressures simultaneously—such as predicting the world accurately, selecting effective actions, maintaining internal consistency, generalising from limited information, and minimising cognitive effort. Rather than treating these as separate objectives, we combine them into a single scalar potential,

$$J(\eta) = J_{\text{prediction}}(\eta) + J_{\text{complexity}}(\eta) + J_{\text{reward}}(\eta) + J_{\text{norms}}(\eta) + J_{\text{effort}}(\eta) + \dots,$$

where $J_{\text{prediction}}$ penalises mismatch between internal predictions and observations, $J_{\text{complexity}}$ penalises unnecessary representational or structural complexity, J_{reward} captures task utility or goal-directed value, J_{norms} encodes logical, social, or consistency constraints, J_{effort} reflects computational or attentional costs, and \dots indicates that additional task- or domain-specific components may be included. Together, these components form a unified cognitive potential that captures the trade-offs inherent to cognition. The smoothness of J ensures that its gradient and curvature are well defined, laying the foundation for the geometric gradient-flow framework developed below.

2.2 Metric and gradient flow

To describe how the cognitive state evolves over time, we endow the cognitive manifold with a geometry that specifies which directions in state space are easy or difficult to move through. This geometry is encoded by a Riemannian metric,^{20,21} which in our formulation is represented in coordinates by a positive-definite matrix that may vary with the state.

Definition 2 (Metric and Riemannian gradient flow). *For each $\eta \in \mathbb{R}^n$, let*

$$G(\eta) = \begin{pmatrix} g_{11}(\eta) & g_{12}(\eta) & \cdots & g_{1n}(\eta) \\ g_{21}(\eta) & g_{22}(\eta) & \cdots & g_{2n}(\eta) \\ \vdots & \vdots & \ddots & \vdots \\ g_{n1}(\eta) & g_{n2}(\eta) & \cdots & g_{nn}(\eta) \end{pmatrix} \in \mathbb{R}^{n \times n},$$

a symmetric, positive-definite matrix whose entries encode the local geometric structure of the cognitive manifold. The Riemannian gradient flow of the cognitive potential J with respect to this metric is defined by

$$\frac{d\eta}{dt} = -G(\eta)^{-1} \nabla_{\eta} J(\eta). \quad (1)$$

The metric $G(\eta)$ determines how changes in different directions of the cognitive states are scaled or weighted. By definition, a Riemannian metric must be symmetric and positive-definite, ensuring that it defines a valid inner product, assigns positive lengths to all nonzero directions, and yields well-posed gradient-flow dynamics. These conditions guarantee that every possible change of state has a strictly positive geometric “cost,” that angles and distances are well defined, and that $G(\eta)^{-1}$ exists so the gradient flow follows the uniquely determined direction of steepest descent. In Euclidean gradient descent,^{22–24} all directions are treated equivalently, but in cognition, some internal adjustments (such as updating habits or low-level perceptual parameters) may be easier or faster than others (such as revising long-term beliefs, engaging working memory, or performing deliberative reasoning). By allowing $G(\eta)$ to vary across the state space, we capture this heterogeneity: the inverse metric $G(\eta)^{-1}$ amplifies directions that are easy to modify and attenuates those that are cognitively costly.

The Riemannian gradient. In a curved or anisotropic geometry, the notion of “steepest descent” is no longer defined by the Euclidean inner product but by the geometric inner product

$$\langle a, b \rangle_G = a^T G(\eta) b, \quad a, b \in \mathbb{R}^n.$$

Because the gradient is defined through the inner product, replacing the Euclidean inner product with the metric-induced one ensures that “steepest descent” is computed relative to the cognitive geometry encoded by $G(\eta)$. The Riemannian gradient $\nabla^{(G)}J$ is the unique vector field satisfying

$$\langle \nabla^{(G)}J(\eta), v \rangle_G = dJ(v) \quad \text{for all directions } v,$$

where $dJ(v)$ is the directional derivative of J along v . Solving this relation yields the explicit expression

$$\nabla^{(G)}J(\eta) = G(\eta)^{-1}\nabla_\eta J(\eta),$$

so that the gradient flow (1) can be written succinctly as

$$\dot{\eta} = -\nabla^{(G)}J(\eta).$$

where $\dot{\eta}$ denotes the time derivative of the cognitive state.

The resulting dynamical law (1) is the coordinate expression of the Riemannian gradient flow on the cognitive manifold. It formalises cognition as the continuous movement of the internal state $\eta(t)$ in the direction that most rapidly decreases the cognitive potential $J(\eta)$, while respecting the geometric structure imposed by $G(\eta)$. This geometric formulation allows representational constraints, resource limitations, and structural relations between cognitive variables to be incorporated directly into the dynamics.

2.3 Monotonicity of the cognitive potential

A central property of the gradient-flow formulation is that the cognitive potential J decreases monotonically along every trajectory of the dynamics. This means that the internal state $\eta(t)$ moves continuously toward configurations of lower cognitive cost, reflecting the intuition that cognitive processing proceeds by reducing prediction errors, resolving conflicts, simplifying representations, or achieving task-relevant goals. The following proposition applies this intuition in precise mathematical form.

Proposition 1 (Monotonic decrease of the cognitive potential). *Assume $J \in C^1$ and $G(\eta)$ is symmetric positive-definite for all η . Then along any solution $\eta(t)$ of (1),*

$$\frac{d}{dt}J(\eta(t)) \leq 0,$$

with equality if and only if $\nabla_\eta J(\eta(t)) = 0$.

Proof. By the chain rule,

$$\frac{d}{dt}J(\eta(t)) = \nabla_\eta J(\eta(t))^\top \dot{\eta}(t).$$

Substituting the gradient-flow equation (1) yields

$$\frac{d}{dt}J(\eta(t)) = -\nabla_\eta J(\eta(t))^\top G(\eta(t))^{-1}\nabla_\eta J(\eta(t)).$$

Because $G(\eta(t))^{-1}$ is positive-definite, the quadratic form on the right-hand side is nonnegative and vanishes only when $\nabla_\eta J(\eta(t)) = 0$. \square

This result formalises the “downhill” nature of cognitive change implied by the gradient-flow law: the system always evolves in a direction that decreases the cognitive potential, and it comes to rest only at critical points where the gradient of J vanishes. In cognitive terms, these stationary points correspond to internal states in which predictive errors, structural tensions, or competing objectives have been locally reconciled. Thus, the monotonicity of J expresses the principle that cognitive processing progressively reduces incompatibilities or inefficiencies in the agent’s internal representation of the world.

3. Anisotropic geometry and emergent fast–slow cognition

The geometric formulation developed above allows the metric to shape not only the direction but also the characteristic time scales of cognitive dynamics. A particularly important case is when certain directions in the state space are much “easier” for the system to move along than others. Such anisotropy—which can reflect differences in cognitive effort, habitual strength, or representational stiffness—naturally gives rise to two distinct regimes: a fast, automatic adjustment of some variables, and a slow, deliberative evolution of others. This section formalises this phenomenon.

3.1 Fast–slow splitting of the cognitive state

We decompose the cognitive state $\eta \in \mathbb{R}^n$ into two groups of coordinates,

$$\eta = \begin{pmatrix} h \\ c \end{pmatrix}, \quad h \in \mathbb{R}^m, \quad c \in \mathbb{R}^k, \quad m + k = n.$$

This condition ensures that h and c form a complete partition of the cognitive state, so that no degrees of freedom are lost or duplicated. Components in h correspond to aspects of cognition that can be updated cheaply or rapidly (such as intuitive, habitual, or automatic adjustments), whereas those in c correspond to processes that are intrinsically costly or slow to change (such as beliefs, goals, or controlled processes). Although cognition may span a continuum of timescales, the fast–slow decomposition captures the dominant separation: intermediate-speed processes are absorbed into the effective slow dynamics in the singular-perturbation limit. This distinction is not imposed by hand but emerges from the anisotropic metric introduced below.

3.2 Anisotropic metric

To model the difference in update difficulty, we equip the cognitive manifold with a block-diagonal metric that assigns different costs to motion in different directions.

Assumption 1 (Anisotropic metric). *For a fixed small parameter $0 < \varepsilon \ll 1$, define*

$$G_\varepsilon = \begin{pmatrix} I_m & 0 \\ 0 & \varepsilon^{-2} I_k \end{pmatrix}.$$

Motion in the c -directions therefore incurs a cost of order ε^{-2} , much greater than the $O(1)$ cost in the h -directions. Since the Riemannian gradient scales as $G_\varepsilon^{-1} \nabla_\eta J$, the corresponding inverse metric is

$$G_\varepsilon^{-1} = \begin{pmatrix} I_m & 0 \\ 0 & \varepsilon^2 I_k \end{pmatrix}.$$

Writing $\nabla_\eta J = (\nabla_h J, \nabla_c J)$, the gradient flow (1) becomes

$$\begin{aligned} \dot{h} &= -\nabla_h J(h, c), \\ \dot{c} &= -\varepsilon^2 \nabla_c J(h, c). \end{aligned} \tag{2}$$

where \dot{h} and \dot{c} denote the time derivatives of the fast and slow components of the cognitive state $\dot{\eta}$.

Thus, the h -variables evolve on an $O(1)$ time scale, whereas the c -variables evolve on an $O(\varepsilon^2)$ time scale, yielding the canonical fast–slow structure that arises directly from the anisotropic geometry.

3.3 Assumptions on the potential

We impose mild structural conditions on the cognitive potential J to ensure that the fast subsystem is well behaved and that a slow manifold exists.

Assumption 2 (Regularity and stability). (J1) **Smoothness.** $J(h, c)$ is twice continuously differentiable on $\mathbb{R}^m \times \mathbb{R}^k$.

(J2) **Unique fast minimiser.** For each fixed c in an open set $C \subset \mathbb{R}^k$, the function $h \mapsto J(h, c)$ has a unique minimiser $h^*(c)$ satisfying

$$\nabla_h J(h^*(c), c) = 0.$$

(J3) **Strong stability.** There exists $\alpha > 0$ such that for all $c \in C$,

$$\lambda_{\min}(\nabla_{hh}^2 J(h^*(c), c)) \geq \alpha,$$

where $\lambda_{\min}(\cdot)$ denotes the smallest eigenvalue of the Hessian matrix, and the condition $\lambda_{\min} \geq \alpha > 0$ ensures strong convexity and exponential stability of the fast equilibrium.

(J4) **Smooth dependence.** The mapping $c \mapsto h^*(c)$ is continuously differentiable on C .

Together, these conditions guarantee that the fast subsystem converges rapidly to a smooth “valley” of equilibria and that this structure persists when ε is small but nonzero.

3.4 Main theorem

Before presenting the formal result, we outline the intuition. Because the metric assigns very different costs to the h - and c -directions, the gradient flow cannot move uniformly in all coordinates. Trajectories first undergo a rapid adjustment in the h -variables, descending toward the configuration $h^*(c)$ that is optimal for the current value of c . Only after this fast relaxation do the c -variables begin to change, drifting slowly along the manifold of fast equilibria. Geometrically, the potential J forms narrow, steep valleys in the h -directions and broad, shallow slopes in the c -directions; the system falls quickly into a valley and then slides gradually along it. The theorem below formalises this picture.

Theorem 1 (Fast–slow decomposition of an anisotropic gradient flow). *Consider the system (2) with $0 < \varepsilon \ll 1$ under Assumptions (J1)–(J4). Define the critical manifold*

$$\mathcal{M}_0 = \{(h, c) \in \mathbb{R}^m \times C : \nabla_h J(h, c) = 0\} = \{(h^*(c), c) : c \in C\}.$$

Then the following statements hold.

(1) **Fast relaxation of h .** For each fixed c , the fast subsystem

$$\dot{h} = -\nabla_h J(h, c)$$

has a unique exponentially stable equilibrium $h^*(c)$, and trajectories converge to this equilibrium on an $O(1)$ time scale.

(2) **Existence of a slow manifold.** There exists $\varepsilon_0 > 0$ such that for all $0 < \varepsilon < \varepsilon_0$, the full system admits a locally invariant manifold

$$\mathcal{M}_\varepsilon = \{(h, c) : h = h^*(c) + O(\varepsilon^2)\},$$

which attracts nearby trajectories on the fast time scale and lies $O(\varepsilon^2)$ -close to \mathcal{M}_0 .

(3) **Reduced slow dynamics.** Restricted to \mathcal{M}_ε , the slow variables evolve as

$$\dot{c} = -\varepsilon^2 \nabla_c J(h^*(c), c) + O(\varepsilon^3),$$

and therefore change on an $O(\varepsilon^2)$ time scale.

(4) **Interpretation.** The gradient flow decomposes into:

- a fast, automatic relaxation of the h -variables toward $h^*(c)$, and
- a slow evolution of the c -variables along \mathcal{M}_ε .

Both behaviours arise from the same geometric law and require no modular or dual-process assumptions.

4. Proof of Theorem 1 (step by step)

We outline a standard argument from fast–slow dynamical systems theory using singular perturbation methods (Tikhonov and Fenichel theory). The proof follows the classical structure: we analyse the fast subsystem, identify the critical manifold, verify normal hyperbolicity, and apply Fenichel’s persistence theorem, and derive the reduced slow dynamics. For clarity, we present the argument in five intuitive steps.

Step 1: Fast subsystem and stability of $h^*(c)$.

Fix any $c \in C$ and consider the fast subsystem

$$\dot{h} = -\nabla_h J(h, c).$$

By Assumption (J2), there is a unique equilibrium $h^*(c)$ satisfying

$$\nabla_h J(h^*(c), c) = 0.$$

Linearising about $h^*(c)$ gives the evolution of perturbations around the equilibrium. Here δh denotes a small deviation from $h^*(c)$, so that linearising the dynamics corresponds to studying how these deviations evolve. This yields

$$\delta \dot{h} = -\nabla_{hh}^2 J(h^*(c), c) \delta h.$$

Assumption (J3) states that all eigenvalues of $\nabla_{hh}^2 J(h^*(c), c)$ are $\geq \alpha > 0$, so all eigenvalues of $-\nabla_{hh}^2 J$ are $\leq -\alpha < 0$. Thus $h^*(c)$ is an exponentially stable equilibrium, with uniform convergence rate at least α .

This proves item (1) of the theorem.

Step 2: The critical manifold and normal hyperbolicity.

Define the set of equilibria of the fast subsystem:

$$\mathcal{M}_0 = \{(h, c) : \nabla_h J(h, c) = 0\} = \{(h^*(c), c) : c \in C\}.$$

By Assumption (J4), the mapping $c \mapsto h^*(c)$ is C^1 , so \mathcal{M}_0 is a smooth embedded manifold.

Consider the full system

$$\dot{h} = -\nabla_h J(h, c), \quad \dot{c} = -\varepsilon^2 \nabla_c J(h, c).$$

Setting $\varepsilon = 0$ freezes the c -variables:

$$\dot{h} = -\nabla_h J(h, c), \quad \dot{c} = 0.$$

On \mathcal{M}_0 , the Jacobian in the h -direction is

$$-\nabla_{hh}^2 J(h^*(c), c),$$

whose eigenvalues are strictly negative by Assumption (J3). In contrast, the linearisation in the c -direction satisfies

$$\delta \dot{c} = 0,$$

so the corresponding eigenvalues are zero. Hence \mathcal{M}_0 is a normally hyperbolic attracting manifold: it attracts trajectories exponentially fast in the h -directions while remaining neutral in the c -directions. Normal hyperbolicity is precisely the condition required for the persistence results in Fenichel's theorem.

Step 3: Persistence of the slow manifold for small ε .

Fenichel's theorem states that normally hyperbolic invariant manifolds persist under sufficiently small perturbations. Thus, there exists $\varepsilon_0 > 0$ such that for all $0 < \varepsilon < \varepsilon_0$, the full system admits a locally invariant manifold

$$\mathcal{M}_\varepsilon = \{(h, c) : h = h^*(c) + O(\varepsilon)\},$$

which is $O(\varepsilon)$ -close to \mathcal{M}_0 and attracts nearby trajectories on the fast time scale.

This proves item (2) of the theorem.

Step 4: Reduced slow dynamics on \mathcal{M}_ε .

On \mathcal{M}_ε we have

$$h = h^*(c) + O(\varepsilon),$$

so substituting into the slow equation gives

$$\dot{c} = -\varepsilon^2 \nabla_c J(h^*(c) + O(\varepsilon), c).$$

Expanding $\nabla_c J(h, c)$ in h around $h^*(c)$ and using $h - h^*(c) = O(\varepsilon)$ yields

$$\nabla_c J(h^*(c) + O(\varepsilon), c) = \nabla_c J(h^*(c), c) + O(\varepsilon),$$

and therefore

$$\dot{c} = -\varepsilon^2 \nabla_c J(h^*(c), c) + O(\varepsilon^3).$$

Thus c evolves according to a reduced gradient flow on an $O(\varepsilon^2)$ time scale. This proves item (3) of the theorem.

Final observation. Steps (1)–(4) together show that the dynamics separate cleanly into two regimes: a fast relaxation in the h -variables toward $h^*(c)$, followed by a slow evolution of the c -variables along the perturbed manifold \mathcal{M}_ε . These behaviours arise from a single anisotropic gradient flow, completing the proof. \square

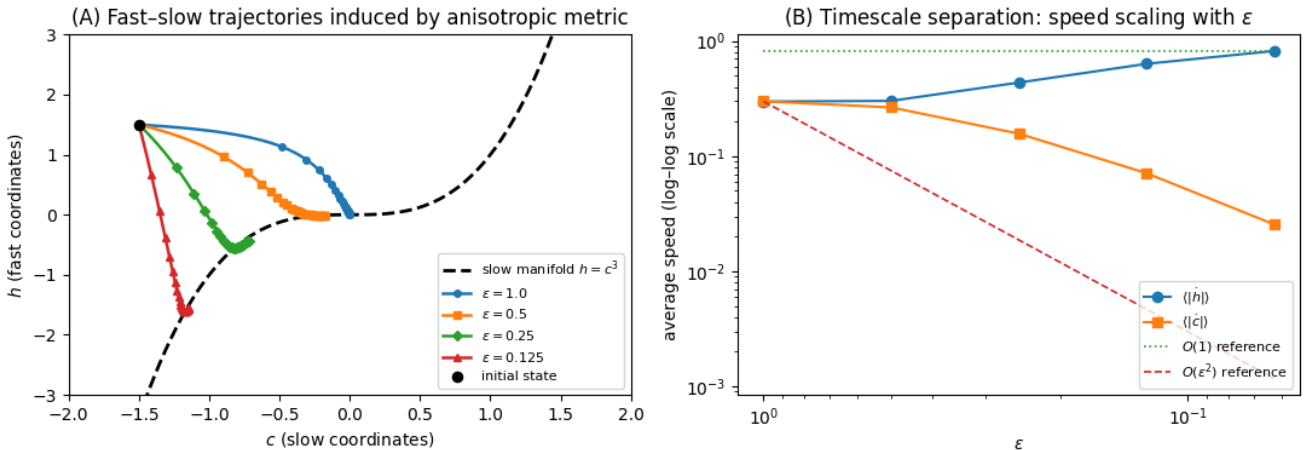


Figure 2. Numerical verification of Assumption 1 (anisotropic metric). (A) Phase portrait of trajectories for multiple values of ϵ under the gradient flow $\dot{h} = -\nabla_h J(h, c)$, $\dot{c} = -\epsilon^2 \nabla_c J(h, c)$. Trajectories rapidly relax toward the slow manifold $h = c^3$ (black dashed) in the h -direction before drifting slowly in the c -direction. Decreasing ϵ sharpens this separation of timescales. (B) Scaling of the average speeds $\langle |\dot{h}| \rangle$ and $\langle |\dot{c}| \rangle$ as functions of ϵ . The empirical curves follow the predicted asymptotic behavior: $\langle |\dot{h}| \rangle \sim O(1)$ and $\langle |\dot{c}| \rangle \sim O(\epsilon^2)$, directly confirming the effect of the anisotropic metric on the Riemannian gradient flow.

Results

The following results illustrate how the proposed geometric framework gives rise to fast–slow cognitive dynamics, stable manifold structure, and accurate low-dimensional reductions, and how these mathematical properties manifest in behaviourally meaningful phenomena. We begin by examining a simple two-dimensional potential that makes the timescale separation induced by the anisotropic metric directly visible. We then test the regularity and stability conditions required for the existence of a slow manifold, and quantify the accuracy of the reduced dynamics predicted by the main theorem. Finally, we demonstrate how the same geometric principles reproduce hallmark features of human decision making, including rapid automatic responses, gradual deliberative drift, and abrupt context-dependent switching. These simulations collectively provide an interpretable visualisation of the geometry and dynamics underlying the theoretical results.

To illustrate how the anisotropic geometry shapes the dynamics of the cognitive gradient flow, we begin with a simple two-dimensional potential

$$J(h, c) = \frac{1}{2}(h - c^3)^2 + \frac{1}{2}c^2,$$

which provides an interpretable setting in which the fast and slow coordinates can be visualised directly. The gradients of this potential are $\nabla_h J = h - c^3$ and $\nabla_c J = (h - c^3)(-3c^2) + c$, so when the system evolves under the anisotropic metric G_ϵ , motion in the fast direction h proceeds with $O(1)$ speed, whereas motion in the deliberative direction c is slowed by a factor of ϵ^2 . The resulting gradient flow,

$$\dot{h} = -\nabla_h J(h, c), \quad \dot{c} = -\epsilon^2 \nabla_c J(h, c),$$

therefore provides a clear example of the mechanism behind Assumption 1: steep energetic directions generate rapid automatic adjustments, while shallow directions produce much slower deliberative evolution. This model serves as a minimal testbed for examining timescale separation, the emergence of a slow manifold, and the accuracy of the reduced dynamics.

Figure 2 empirically verifies this prediction. Panel (A) shows trajectories in the (c, h) -plane for several values of ϵ , together with the slow manifold $h = c^3$. For each ϵ , the h -coordinate collapses rapidly toward the manifold, while the c -coordinate drifts slowly along it. As ϵ decreases, this collapse becomes sharper, illustrating the emergence of fast relaxation in the h -directions. Panel (B) reports the average magnitudes of $\langle |\dot{h}| \rangle$ and $\langle |\dot{c}| \rangle$ over time on a log–log scale. The speed in the h -coordinates remains approximately constant ($O(1)$), whereas the speed in the c -coordinates scales quadratically in ϵ , matching the theoretical scaling $\langle |\dot{c}| \rangle = O(\epsilon^2)$. The empirical curves align closely with the reference slopes. Together, these results provide a direct numerical demonstration that the anisotropic metric indeed generates a fast–slow dynamical structure, validating Assumption 1.

A central requirement of our framework is that automatic cognitive components rapidly stabilize around a context-dependent configuration determined by the current deliberative or goal-directed state. Assumption 2 formalizes this idea by requiring

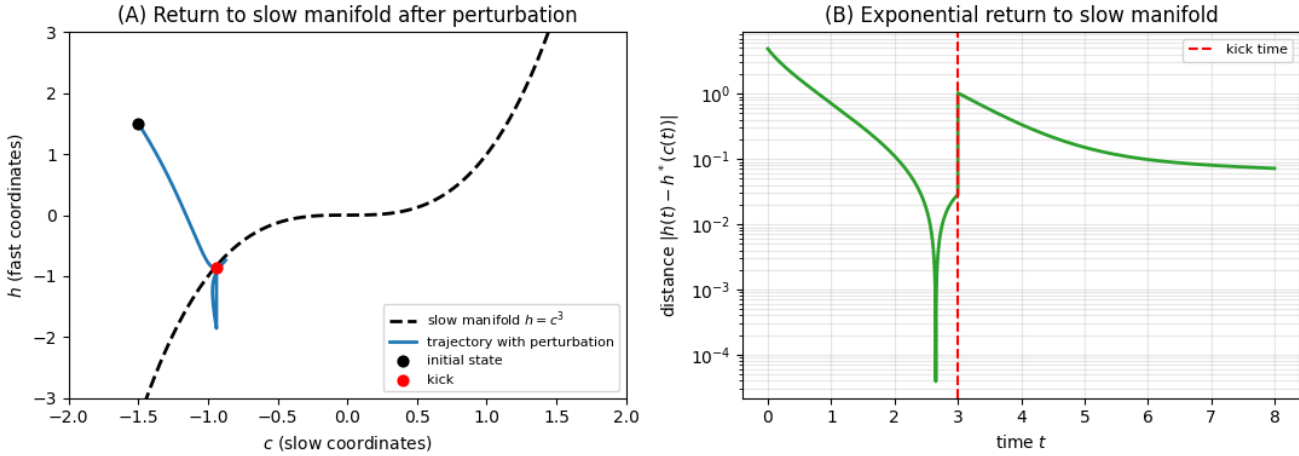


Figure 3. Numerical illustration of Assumption 2 (Regularity and Stability) in a cognitive fast–slow system. (A)

Trajectory of the full cognitive gradient flow under the anisotropic metric, shown together with the slow manifold $h^*(c) = c^3$ (black dashed), which represents the stable equilibrium of the fast, automatic cognitive coordinates for each deliberative state c . From the initial condition (black), the system rapidly relaxes toward this manifold in the automatic coordinate h , while the deliberative coordinate c changes only slowly. At time t_{kick} (red), we artificially perturb the automatic state by adding a displacement to h . Despite this disruption, the trajectory quickly returns to $h^*(c)$, demonstrating that the automatic subsystem possesses a unique, robustly attracting equilibrium for each fixed c , as required by Assumption 2. **(B)** Distance to the slow manifold, $D(t) = |h(t) - h^*(c(t))|$, plotted on a semilogarithmic scale. Both before and after the perturbation, $D(t)$ decays nearly exponentially, indicating strong local contraction in the fast directions and verifying the stability conditions specified in Assumption 2. Together, these panels show that automatic cognitive states reliably and rapidly settle into context-dependent equilibria, enabling well-defined reduced dynamics for the slower deliberative variables.

that for every deliberative state c , the automatic subsystem in h possesses a unique and strongly attracting equilibrium $h^*(c)$ representing the habitual or reflexive response most compatible with that context. Figure 3 illustrates this mechanism. The trajectory shows an initial rapid convergence of h toward the manifold $h = c^3$, corresponding to the formation of an automatic response pattern. When an external perturbation briefly disrupts h , the system quickly restores the appropriate automatic configuration, while the deliberative variable c changes only gradually. This robust, near-exponential return to equilibrium demonstrates that automatic processes are stable and self-correcting, enabling deliberative processes to evolve coherently over longer timescales. These observations empirically validate the regularity and stability assumptions that justify the reduced cognitive dynamics derived in our theory.

The numerical simulations illustrate the geometric mechanisms underlying the fast–slow decomposition and the validity of the manifold-based reduction, as shown in Figure 4 and 5. When the system evolves under the anisotropic metric, the fast coordinate rapidly relaxes toward the context-dependent equilibrium $h^*(c)$, while the slow coordinate drifts gradually according to its much weaker effective gradient. This rapid convergence ensures that, after a brief transient, trajectories remain close to the slow manifold defined by the minimizers of J with respect to h . The reduced dynamics obtained by restricting the flow to this manifold closely match the evolution of the slow variables in the full system, and the maximal deviation between the two decays systematically as the timescale separation parameter ε decreases, in agreement with the theoretical predictions. Together, these numerical results demonstrate that the full cognitive gradient flow contracts strongly in the fast directions, quickly aligning the automatic state with the current deliberative context, and subsequently evolves in a lower-dimensional space governed by the reduced slow dynamics. This behavior provides empirical support for the regularity, stability, and reduction assumptions that form the foundation of the theoretical framework.

To illustrate how the proposed geometric framework captures core features of human decision making, we simulated a simple two-choice task in which an agent must choose between two competing interpretations while gradually receiving evidence (Figure 6). In this model, the fast coordinate h represents automatic, habitual, or intuitive responses—those that stabilize quickly and require minimal cognitive effort—whereas the slow coordinate c captures deliberative or reflective processing that integrates information over longer timescales. The cognitive potential $J(h, c, t)$ defines a dynamic decision landscape whose shape encodes both internal preferences and the structure of the external environment. Early in the trial, the landscape contains two comparable decision basins, reflecting uncertainty between alternatives. As additional evidence accumulates, the landscape deforms, biasing the deliberative state toward a new attractor.

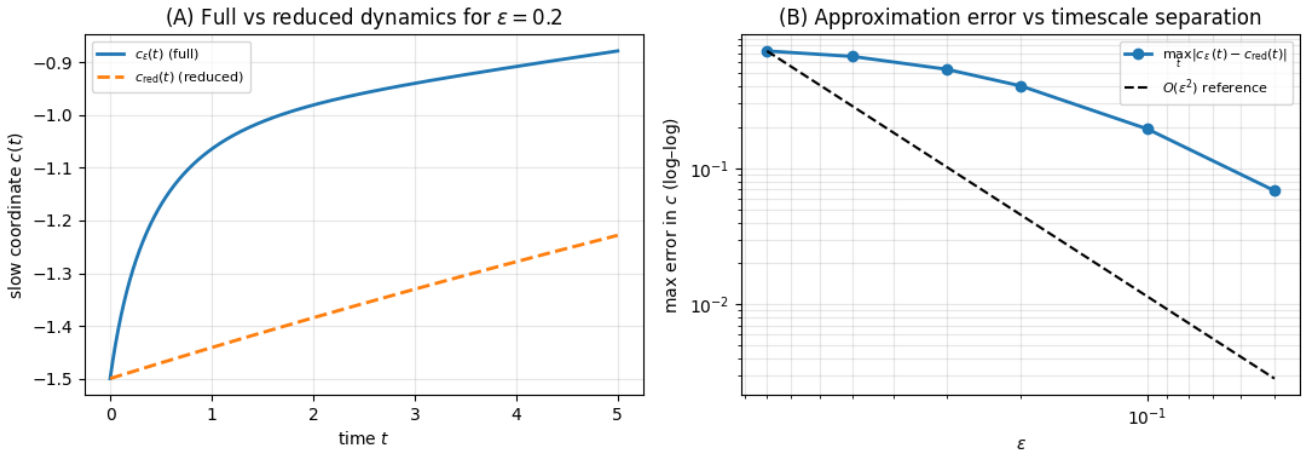


Figure 4. Numerical validation of the reduced slow dynamics. (A) Comparison of the slow coordinate obtained from the full fast-slow system $c_\varepsilon(t)$ and from the reduced dynamics $c_{\text{red}}(t)$ defined on the slow manifold $h^*(c) = c^3$, shown here for $\varepsilon = 0.2$. After an initial transient during which the fast coordinate rapidly equilibrates, the slow variable of the full system evolves closely to the reduced trajectory, illustrating the accuracy of the manifold-based reduction. (B) Maximum-in-time error between the full and reduced slow variables, $\max_t |c_\varepsilon(t) - c_{\text{red}}(t)|$, plotted as a function of ε on a log-log scale. The error decreases systematically as $\varepsilon \rightarrow 0$ and follows an approximately quadratic scaling, consistent with the theoretical prediction for the accuracy of the reduced dynamics. Together, these results empirically confirm the main reduction theorem and demonstrate that the slow evolution of the full cognitive gradient flow is well-approximated by the dynamics on the slow manifold.

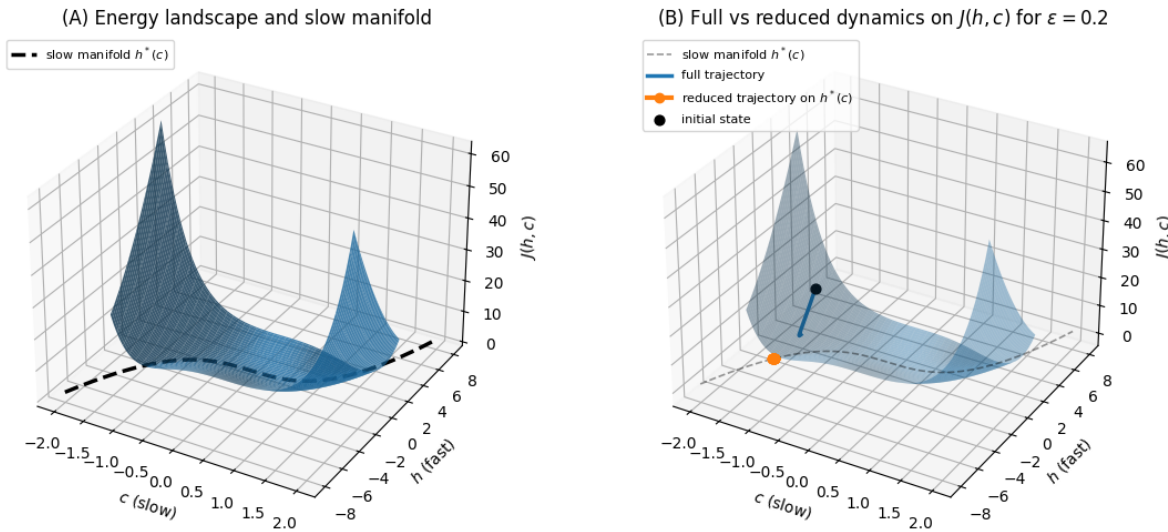


Figure 5. Geometric structure of the cognitive potential and validation of the reduced dynamics. (A) Energy landscape $J(h, c)$ for the two-dimensional illustrative system, shown as a smooth surface over the fast coordinate h and slow coordinate c . The black dashed curve marks the slow manifold $h^*(c) = c^3$, which corresponds to the unique minimizer of J with respect to h for each fixed c . This curve forms a stable valley in the landscape and represents the equilibrium configuration of the fast, automatic cognitive variables conditioned on the deliberative state c . (B) Full trajectory of the anisotropic gradient flow (blue), projected into the energy landscape. After an initial transient, the trajectory rapidly contracts toward the slow manifold and then evolves along it. The reduced trajectory (orange dashed), obtained by restricting the dynamics to $h^*(c)$, closely matches the full system once it has entered the valley. The initial state is shown in black. Together, the two panels demonstrate that the fast subsystem stabilizes on $h^*(c)$ and that the slow evolution of the full system is accurately captured by the reduced dynamics, providing geometric intuition and numerical support for the main reduction theorem.

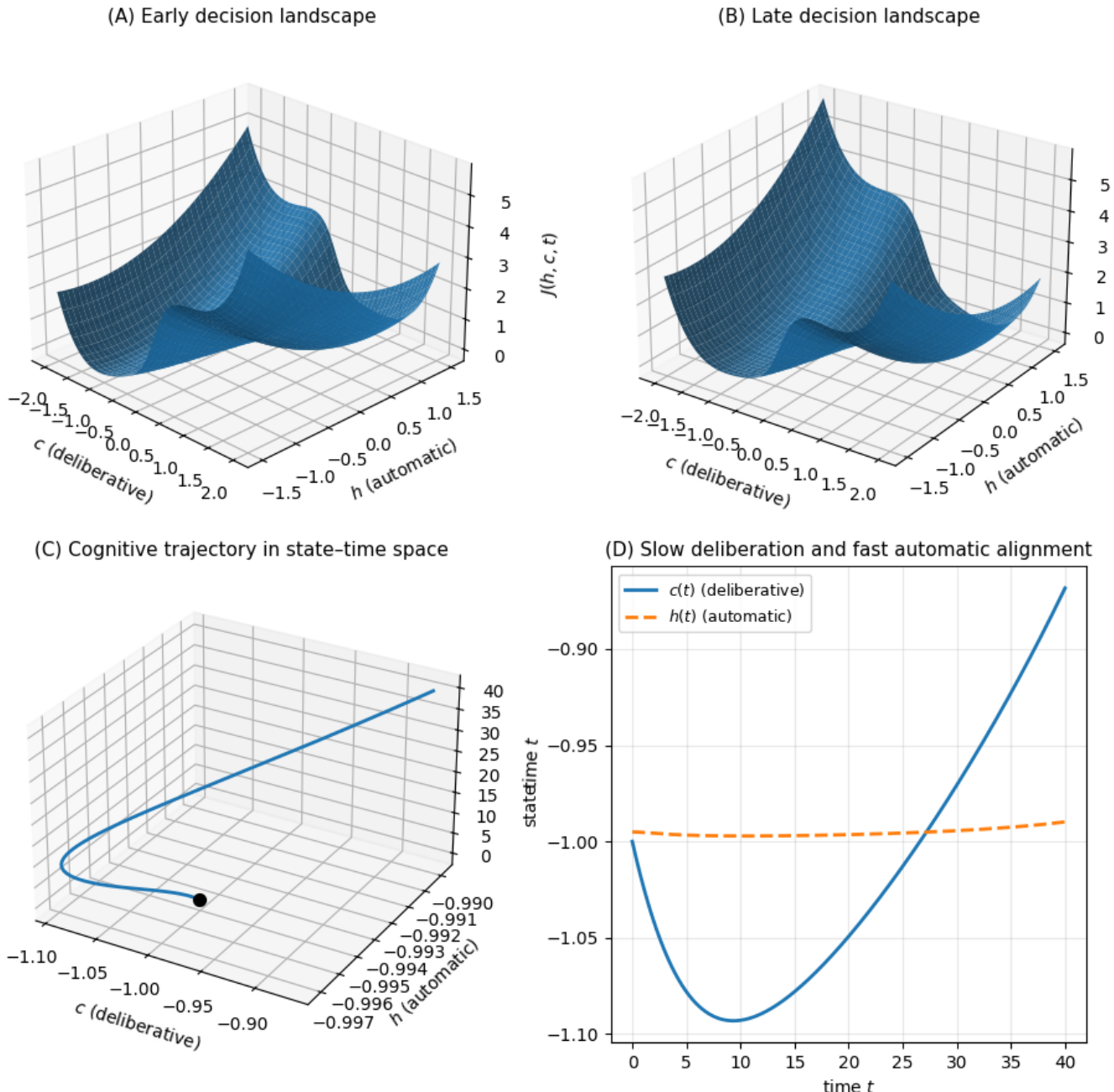


Figure 6. Cognitive gradient flow illustrating fast automatic responses and slow deliberative dynamics. (A) Early decision landscape $J(h, c, t)$ showing two approximately symmetric basins in the deliberative coordinate c , each corresponding to a stable decision mode. (B) As external evidence gradually shifts, the energy landscape deforms and one basin deepens, biasing the system toward an alternative decision. (C) Trajectory of the full gradient flow in (c, h, t) space. The automatic variable h rapidly aligns with the instantaneous habitual response $g(c)$, while the deliberative variable c evolves slowly until crossing the unstable saddle and switching decisional mode. (D) Time courses of the two coordinates highlight the timescale separation: $h(t)$ responds quickly and remains close to $g(c)$, whereas $c(t)$ drifts gradually and undergoes a discrete transition when the landscape reconfigures. Together, the panels demonstrate how a single anisotropic gradient flow naturally produces dual-process behaviour, with fast automatic adjustments emerging from steep energetic directions and slower deliberation driven by shallow geometric structure in the cognitive potential.

The resulting dynamics exhibit hallmark signatures of dual-process cognition. The automatic state h adapts rapidly to the context set by c , remaining close to the intuitive response $g(c)$ at nearly all times. In contrast, the deliberative variable c drifts slowly across the landscape, moving through a shallow energetic valley until sufficient evidence causes it to cross a stability threshold and commit to an alternative interpretation. This produces a characteristic “tipping point” dynamic: gradual accumulation followed by a sudden decision switch, after which the automatic state realigns almost immediately with the new goal. Together, these simulations demonstrate how a single gradient-flow mechanism, endowed with anisotropic geometry, naturally generates fast intuitive behavior, slow deliberative updating, context-dependent choice transitions, and rapid realignment of automatic processes following changes in belief.

Implications for Cognitive Science and AGI

The geometric framework developed here provides a unified lens through which to understand both human cognition and the design of artificial agents. Expressing cognitive dynamics as the Riemannian gradient flow

$$\dot{\eta}(t) = -G(\eta)^{-1}\nabla J(\eta)$$

yields four central insights about natural and artificial intelligence.

First, the framework unifies a wide range of existing cognitive and computational theories. Bayesian inference, predictive coding, reinforcement learning, deep representation learning, the free-energy principle, and dual-process accounts of intuition and deliberation all emerge as special cases of gradient flow under different choices of potential J and metric G . This provides a mathematical explanation for the empirical success of these models and clarifies their relationships: rather than being competing theories, they can be interpreted as different parameterisations of a single underlying geometric principle governing learning and decision dynamics.

Second, the model predicts new psychological phenomena. Variations in the metric $G(\eta)$ and curvature $\nabla^2 J(\eta)$ give rise to systematic differences in cognitive effort, working-memory load, attention allocation, heuristics, and the difficulty of overriding habitual responses. Because the formulation defines a continuous dynamical system, it generates trajectory-level predictions about learning curves, response times, switching between intuitive and deliberative modes, and susceptibility to noise or stress—phenomena traditionally modelled separately.

Third, the framework offers a principled basis for designing artificial general intelligence. Representing an agent’s internal configuration as a latent cognitive state η , updated through the gradient flow of a unified potential J , subsumes both deep learning^{25,26} and reinforcement learning^{27–29} within a common geometric description. Learning corresponds to shaping the potential and metric through data, while decision-making corresponds to following the induced flow. This perspective avoids modular architectures separating memory, prediction, reward, and planning. Many recent approaches—world models,^{30,31} JEPA-style self-supervised systems,³² GFlowNets,³³ and differentiable decision-making³⁴ pipelines—can be viewed as concrete instances of this formulation. The anisotropic metric naturally induces fast intuitive and slow deliberative processes, enabling agents to allocate computational resources adaptively and to reason over multiple time scales.

Finally, the geometric structure of the model provides stability and interpretability advantages that address key limitations of current large-scale neural systems. Gradient flow on a curved manifold ensures smooth transitions between internal states, principled convergence behaviour, and structured long-horizon reasoning trajectories. By integrating a latent cognitive state, a global potential, and a Riemannian geometry, the framework provides a pathway for constructing agents capable of modelling preferences, maintaining coherent goals, and producing behaviour that is robust, predictable, and aligned.

Together, these implications suggest that a geometric perspective on cognition may unify diverse psychological theories and provide a mathematically grounded foundation for the next generation of artificial general intelligence systems.

Conclusion

In summary, we have introduced a geometric framework that unifies a wide class of cognitive processes by modelling internal computation as gradient flow on a cognitive manifold endowed with an anisotropic metric. This formulation identifies fast automatic responses and slow deliberative updates as consequences of the underlying geometry rather than as distinct mechanisms, and establishes conditions under which the resulting dynamics admit a principled low-dimensional reduction. Through a combination of theoretical analysis and targeted simulations, we demonstrated how timescale separation, manifold stability, and reduced dynamics arise naturally from the structure of the potential, and how these mathematical properties give rise to behavioural signatures associated with dual-process cognition, including rapid habitual alignment, gradual evidence integration, and abrupt context-dependent switching.

More broadly, the framework suggests a path toward integrating symbolic, probabilistic, and neural models within a single geometric perspective, and offers a foundation for developing mechanistic accounts of complex cognitive phenomena using tools from differential geometry and dynamical systems. By grounding both intuitive and deliberative behaviour in a common

set of principles, this approach provides a step toward a unified quantitative theory of cognition and offers new opportunities for building artificial systems that mirror the flexibility, stability, and multiscale structure of human thought.

Code availability

Source code on Github: <https://github.com/ainilaha/cognitive-gradient-flows>

References

1. Gornet, J. & Thomson, M. Automated construction of cognitive maps with visual predictive coding. *Nat. Mach. Intell.* **6**, 820–833, DOI: [10.1038/s42256-024-00863-1](https://doi.org/10.1038/s42256-024-00863-1) (2024).
2. Epstein, R. A., Patai, E. Z., Julian, J. B. & Spiers, H. J. The cognitive map in humans: spatial navigation and beyond. *Nat. Neurosci.* **20**, 1504–1513, DOI: [10.1038/nn.4656](https://doi.org/10.1038/nn.4656) (2017).
3. Wimmer, G. E., Liu, Y., Vehar, N., Behrens, T. E. J. & Dolan, R. J. Episodic memory retrieval success is associated with rapid replay of episode content. *Nat. Neurosci.* **23**, 1025–1033, DOI: [10.1038/s41593-020-0649-z](https://doi.org/10.1038/s41593-020-0649-z) (2020).
4. Betteti, S., Baggio, G., Bullo, F. & Zampieri, S. Input-driven dynamics for robust memory retrieval in Hopfield networks. *Sci. Adv.* **11**, eadu6991, DOI: [10.1126/sciadv.adu6991](https://doi.org/10.1126/sciadv.adu6991) (2025).
5. Mnih, V. *et al.* Human-level control through deep reinforcement learning. *Nature* **518**, 529–533, DOI: [10.1038/nature14236](https://doi.org/10.1038/nature14236) (2015).
6. Hafner, D., Pasukonis, J., Ba, J. & Lillicrap, T. Mastering diverse control tasks through world models. *Nature* **640**, 647–653, DOI: [10.1038/s41586-025-08744-2](https://doi.org/10.1038/s41586-025-08744-2) (2025).
7. Pramod, R. T., Mieczkowski, E., Fang, C., Tenenbaum, J. & Kanwisher, N. Decoding predicted future states from the brain’s ‘physics engine’. *J. Vis.* **24**, 1258, DOI: [10.1167/jov.24.10.1258](https://doi.org/10.1167/jov.24.10.1258) (2024).
8. Collins, K. M. *et al.* Building machines that learn and think with people. *Nat. Hum. Behav.* **8**, 1851–1863, DOI: [10.1038/s41562-024-01991-9](https://doi.org/10.1038/s41562-024-01991-9) (2024).
9. Gao, T., Baker, C. L., Tang, N., Xu, H. & Tenenbaum, J. B. The Cognitive Architecture of Perceived Animacy: Intention, Attention, and Memory. *Cogn. Sci.* **43**, 1–31, DOI: [10.1111/cogs.12775](https://doi.org/10.1111/cogs.12775) (2019).
10. Lake, B. M., Ullman, T. D., Tenenbaum, J. B. & Gershman, S. J. Building machines that learn and think like people. *Behav. Brain Sci.* **40**, e253, DOI: [10.1017/S0140525X16001837](https://doi.org/10.1017/S0140525X16001837) (2017).
11. Lake, B. M., Salakhutdinov, R. & Tenenbaum, J. B. Human-level concept learning through probabilistic program induction. *Science* **350**, 1332–1338, DOI: [10.1126/science.aab3050](https://doi.org/10.1126/science.aab3050) (2015). <https://www.science.org/doi/pdf/10.1126/science.aab3050>.
12. Papadimitriou, C. H., Vempala, S. S., Mitropolsky, D., Collins, M. & Maass, W. Brain computation by assemblies of neurons. *Proc. Natl. Acad. Sci.* **117**, 14464–14472, DOI: [10.1073/pnas.2001893117](https://doi.org/10.1073/pnas.2001893117) (2020).
13. Kar, K., Kubilius, J., Schmidt, K., Issa, E. B. & DiCarlo, J. J. Evidence that recurrent circuits are critical to the ventral stream’s execution of core object recognition behavior. *Nat. Neurosci.* **22**, 974–983, DOI: [10.1038/s41593-019-0392-5](https://doi.org/10.1038/s41593-019-0392-5) (2019).
14. Kahneman, D. *Thinking, Fast and Slow* (Farrar, Straus and Giroux, New York: New York, 2011).
15. Riemann, B. On the Hypotheses Which Lie at the Bases of Geometry. *Nature* **8**, 14–17, DOI: [10.1038/008014a0](https://doi.org/10.1038/008014a0) (1873).
16. Lu, M. A mathematical framework of intelligence and consciousness based on riemannian geometry (2024). [2407.11024](https://doi.org/10.4236/240711024).
17. Lee, B. K. *et al.* A principal odor map unifies diverse tasks in olfactory perception. *Science* **381**, 999–1006, DOI: [10.1126/science.ade4401](https://doi.org/10.1126/science.ade4401) (2023).
18. Muttenthaler, L. *et al.* Aligning machine and human visual representations across abstraction levels. *Nature* **647**, 349–355, DOI: [10.1038/s41586-025-09631-6](https://doi.org/10.1038/s41586-025-09631-6) (2025). [2409.06509](https://doi.org/10.1038/s41586-025-09631-6).
19. Griffiths, T. L., Chater, N. & Tenenbaum, J. B. *Bayesian Models of Cognition: Reverse Engineering the Mind* (MIT Press, Boston, MA, 2024).
20. Lebanon, G. Learning riemannian metrics. In *Proceedings of the Nineteenth Conference on Uncertainty in Artificial Intelligence*, UAI’03, 362–369 (Morgan Kaufmann Publishers Inc., San Francisco, CA, USA, 2002).
21. Gruffaz, S., Poulet, P.-E., Maheux, E., Jedyak, B. & DURRLEMAN, S. Learning Riemannian metric for disease progression modeling. In Ranzato, M., Beygelzimer, A., Dauphin, Y., Liang, P. S. & Vaughan, J. W. (eds.) *Advances in Neural Information Processing Systems*, vol. 34, 23780–23792 (Curran Associates, Inc., 2021).

22. Robbins, H. & Monro, S. A stochastic approximation method. *Annals Math. Stat.* **22**, 400–407 (1951).
23. Ruder, S. An overview of gradient descent optimization algorithms. *CoRR* **abs/1609.04747** (2016). [1609.04747](https://arxiv.org/abs/1609.04747).
24. Andrychowicz, M. *et al.* Learning to learn by gradient descent by gradient descent. In *Proceedings of the 30th International Conference on Neural Information Processing Systems*, NIPS’16, 3988–3996 (Curran Associates Inc., Red Hook, NY, USA, 2016).
25. Lecun, Y., Bengio, Y. & Hinton, G. Deep learning. *Nature* **521**, 436–444, DOI: [10.1038/nature14539](https://doi.org/10.1038/nature14539) (2015).
26. He, K., Zhang, X., Ren, S. & Sun, J. Deep residual learning for image recognition. *Proc. IEEE Comput. Soc. Conf. on Comput. Vis. Pattern Recognit.* **2016-Decem**, 770–778, DOI: [10.1109/CVPR.2016.90](https://doi.org/10.1109/CVPR.2016.90) (2016). [1512.03385](https://doi.org/10.1109/CVPR.2016.90).
27. Sutton, R. S. & Barto, A. G. *Reinforcement Learning: An Introduction* (A Bradford Book, Cambridge, MA, USA, 2018).
28. Silver, D. *et al.* Mastering the game of Go with deep neural networks and tree search. *Nature* **529**, DOI: [10.1038/nature16961](https://doi.org/10.1038/nature16961) (2016).
29. Silver, D. *et al.* Mastering the game of Go without human knowledge. *Nature* **550**, 354–359, DOI: [10.1038/nature24270](https://doi.org/10.1038/nature24270) (2017).
30. Wu, J., Yildirim, I., Lim, J. J., Freeman, B. & Tenenbaum, J. Galileo: Perceiving physical object properties by integrating a physics engine with deep learning. In Cortes, C., Lawrence, N., Lee, D., Sugiyama, M. & Garnett, R. (eds.) *Advances in Neural Information Processing Systems*, vol. 28 (Curran Associates, Inc., 2015).
31. LeCun, Y. A path towards autonomous machine intelligence. *Open Rev.* 1–62 (2022).
32. Assran, M. *et al.* V-jepa 2: Self-supervised video models enable understanding, prediction and planning (2025). [2506.09985](https://arxiv.org/abs/2506.09985).
33. Bengio, E., Jain, M., Korablyov, M., Precup, D. & Bengio, Y. Flow network based generative models for non-iterative diverse candidate generation. In Ranzato, M., Beygelzimer, A., Dauphin, Y., Liang, P. & Vaughan, J. W. (eds.) *Advances in Neural Information Processing Systems*, vol. 34, 27381–27394 (Curran Associates, Inc., 2021).
34. Silva, A., Killian, T., Jimenez, I. R., Son, S. H. & Gombolay, M. Optimization Methods for Interpretable Differentiable Decision Trees in Reinforcement Learning. *Proc. Mach. Learn. Res.* **108**, 1855–1865 (2020). [1903.09338](https://arxiv.org/abs/1903.09338).